Effects of turbulence compressibility and unsteadiness in compression corner flow

By A. Brankovic[1] AND O. Zeman[2]

The structure of the separated flow region over a $20°$ compression corner at a free-stream Mach number of 2.84 is investigated computationally using a Reynolds averaged Navier Stokes (R.A.N.S.) solver and $k - \epsilon$ model. At this Mach number and ramp angle, a steady-state recirculation region of order δ_o is observed, with onset of a "plateau" in the wall pressure distribution near the corner. At lower ramp angles, separation is negligible, while at an angle of $24°$, separation regions of length $2\delta_o$ are expected. Of interest here is the response of the mathematical model to inclusion of the pressure dilatation term for turbulent kinetic energy. Compared with the experimental data of Smits and Muck (1987), steady-state computations show improvement when the pressure dilatation term is included. Unsteady computations, using both unforced and then forced inlet conditions, did not predict the oscillatory motion of the separation bubble as observed in laboratory experiments (see e.g. Dolling and Or 1983). An analysis of the separation bubble oscillation and the turbulent boundary layer (T.B.L.) frequencies for this flow suggests that the bubble oscillations are of nearly the same order as the turbulence frequencies, and therefore difficult for the model to separate and resolve.

1. Introduction

The accurate prediction of turbulent, compressible flow at low supersonic speeds ($M_\infty \leq 3$) is one of the most challenging and important problems facing aircraft engine component designers. For rotating components, flows typically feature unsteadiness (periodic and non-periodic) and mild compressibility effects, which when coupled prove difficult to isolate and understand from a fundamental point of view. Analysis of experimental data (Dolling and Or 1983) reveals that even wind tunnel generated flows feature significant flow field unsteadiness, which is difficult to isolate and control. Analysis of the unsteady pressure fluctuations at the foot of the separation shock indicates non-periodic, unsteady movement of the shock foot, with a highly non-Gaussian distribution of the wall pressure fluctuation. Near the bubble "steady-state" separation point where the wall pressure is highly intermittant and where the pressure fluctuations are most intense, the pressure distribution was found to be bi-modal. It was found that the characteristic frequency f_D of the

1 Pratt & Whitney, West Palm Beach, FL
2 Center for Turbulence Research

separation bubble oscillations scales on the incoming boundary layer thickness δ_o and free-stream velocity U_o so that

$$f_D \delta_o / U_o = 0.13.$$

At this resonant frequency, the bubble leading edge moved forward by up to $1.5\delta_o$, doubling its length relative to the steady state value.

Compressibility corrections due to the pressure dilatation for two-equation turbulence models have previously been proposed by Zeman and Coleman (1991) and Horstman (1987). The Zeman-Coleman model was based on the results of a direct numerical simulation (DNS) of turbulence in which the mean flow is subjected to one-dimensional compression; Durbin and Zeman (1992) have formulated a rapid distortion theory which allows calculation of the pressure-dilatation term analytically for cases of rapid compression in one, two, or three directions. Vandromme and Zeman (1992) found that including this term in the $k - \epsilon$ model, using wall integration boundary conditions, significantly improved predictions for $M_\infty = 2.84$ flow over a $24°$ ramp.

In addition to models for the pressure dilatation term, proposals for the dilatation dissipation and turbulence/pressure-gradient interaction terms, turbulent length-scale limiters, and low-Reynolds number corrections for turbulent viscosity have been made for specific features of highly compressible flows (Marvin 1991). Not all of these terms have been tested in mildly compressible flows. The present effort focuses on the evaluation of the pressure dilatation contribution in steady-state predictions of the compression corner flow.

It is noted that model predictions using the standard $k - \epsilon$ model tend to underestimate flow reattachment lengths even in incompressible flows such as backsteps and $180°$ bend ducts. It is ambitious to expect a single turbulence compressibility term to compensate for underlying problems with the model. Nevertheless, it is of great interest to examine whether these terms are important in predicting complex compressible flows, and whether the terms should be generally included in production R.A.N.S. flow solvers.

2. Computational model and solution method

2.1 Governing equations

Computations were performed using the time-dependent form of the compressible R.A.N.S. equations. The continuity, momentum, and energy conservation equations used are shown below:

$$\frac{\partial \rho}{\partial t} + \frac{\partial}{\partial x_j}(\rho U_j) = 0.0 \tag{1}$$

$$\frac{\partial \rho U_i}{\partial t} + \frac{\partial}{\partial x_j}(\rho U_j U_i + \delta_{ij} P - \tau_{ij}) = 0.0 \tag{2}$$

$$\frac{\partial \rho e_t}{\partial t} + \frac{\partial}{\partial x_j}(\rho U_j e_t + P U_j - \tau_{ij} U_i - \frac{\kappa}{C_p}\frac{\partial h}{\partial x_j}) = 0.0 \tag{3}$$

where $P = \rho RT$, $e_t = h - \frac{P}{\rho} + \frac{1}{2}U_j^2$, and $\tau_{ij} = \mu(\frac{\partial U_i}{\partial x_j} + \frac{\partial U_j}{\partial x_i} - \frac{2}{3}\delta_{ij}\frac{\partial U_i}{\partial x_j})$.

The equation set is closed using the Boussinesq approximation for the Reynolds stress tensor:

$$-\rho\overline{u_i u_j} = \mu_t(\frac{\partial U_i}{\partial x_j} + \frac{\partial U_j}{\partial x_i} - \frac{2}{3}\delta_{ij}\nabla \cdot U) - \frac{2}{3}\rho k\delta_{ij} \qquad (4)$$

where the turbulent viscosity is modeled as:

$$\mu_t = C_\mu \rho f_\mu \frac{k^2}{\epsilon} \qquad (5)$$

The turbulent kinetic energy, k and its dissipation rate, ϵ are computed using modeled transport equations:

$$\frac{\partial \rho k}{\partial t} + \frac{\partial \rho U_j k}{\partial x_j} - \frac{\partial}{\partial x_j}(\mu + \frac{\mu_t}{\sigma_k})\frac{\partial k}{\partial x_j} = P - \rho\epsilon + (\overline{p\theta})_R \qquad (6)$$

$$\frac{\partial \rho \epsilon}{\partial t} + \frac{\partial \rho U_j \epsilon}{\partial x_j} - \frac{\partial}{\partial x_j}(\mu + \frac{\mu_t}{\sigma_\epsilon})\frac{\partial \epsilon}{\partial x_j} = C_1 f_1 \frac{\epsilon}{k}P - C_2 f_2 \rho\frac{\epsilon^2}{k} \qquad (7)$$

where $P = -\rho(\overline{u_i u_j})\frac{1}{2}(U_{i,j} + U_{j,i})$, is the production term, and the pressure dilatation term, $\overline{pu_{j,j}} \equiv \overline{p\theta}$, has been added to the R.H.S. of the k equation. Modeling of this term is the subject of the next section. The constants in the turbulence model are the standard values recommended by Jones and Launder (1972), and are $C_\mu = 0.09$, $C_1 = 1.44$, $C_2 = 1.92$, $\sigma_k = 1.0$, $\sigma_\epsilon = 1.30$, $f_\mu = 1.0$, $f_1 = 1.0$ and $f_2 = 1.0$.

2.2 The pressure dilatation model

As the boundary layer turbulence passes through the oblique shock generated by the compression corner, it undergoes a highly rapid compression. This effect is represented by the rapid pressure-dilatation model developed by Zeman (1991) and Zeman and Coleman (1991). The model is based on the physics and theories of rapid distortion and was verified against the DNS of rapidly compressed homogeneous turbulence.

The pressure dilatation term $\overline{p\theta}$ appears on the R.H.S. of the turbulent kinetic energy equation with positive sign. The rapid contribution to $\overline{p\theta}$ proposed by Zeman and co-workers to be tested is

$$(\overline{p\theta})_R = -C_{d1}\overline{\rho}k\tau(S_{ij}^*)^2 \qquad (8)$$

where $S_{ij}^* = \frac{1}{2}(U_{j,i} + U_{i,j} - \frac{2}{3}\delta_{ij}\nabla \cdot U)$ is the trace-free mean strain rate, $\tau = k/\epsilon$ is the turbulent time scale, and $C_{d1} = -0.004$ is the model constant whose value was determined from the DNS computations. For one of the steady-state test runs, a value of $C_{d1} = -0.006$ was used to test the sensitivity of the separation bubble size to this coefficient. It is pointed out that the modeled pressure dilatation term acts as a sink term in the k transport equation and decreases the level of k values wherever it is numerically significant; this is the case in the vicinity of shocks, where mean velocity gradients are steep.
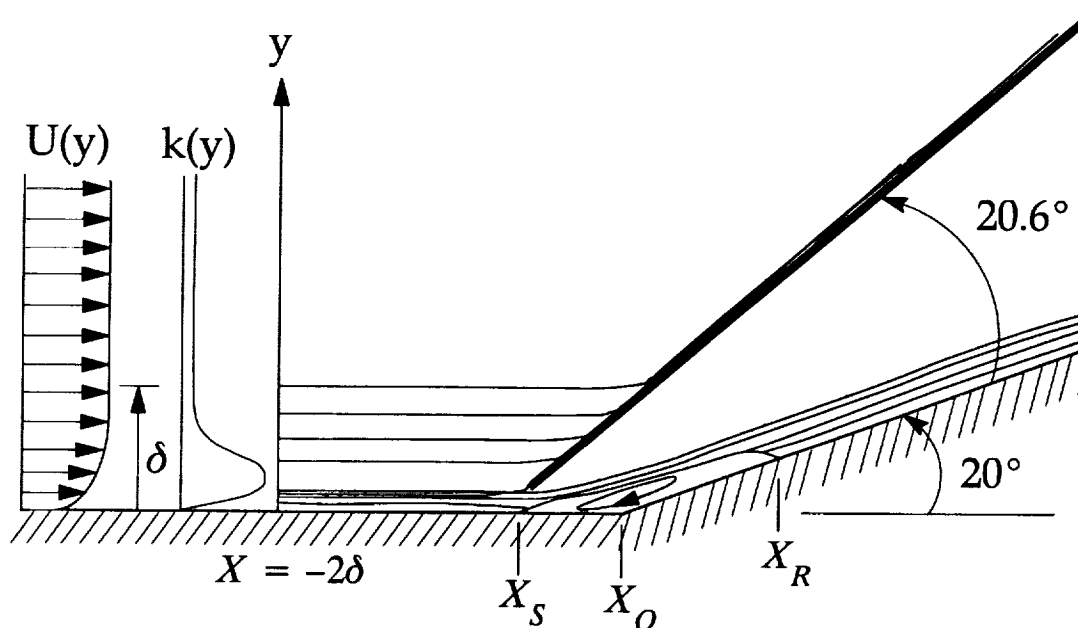
FIGURE 1. Schematic diagram of flow geometry and inlet conditions.

2.3 Numerical method

Computations were done with a code developed at Pratt & Whitney. The equations are transformed to a curvilinear coordinate system and integrated over arbitrary control volumes using a cell-centered grid. A pressure correction procedure is adapted to generalized coordinates. Second and third-order spatial discretization schemes are used interchangeably. A second-order backward temporal scheme is used for the time-dependent calculations.

Inflow conditions consisted of interpolated axial velocity and turbulent kinetic energy profiles obtained from measurements in Smits and Muck (1987). The inlet turbulence dissipation rate and the turbulent viscosity distribution were obtained from the boundary layer distributions given in Hinze (1975). The computational grid was 241 (axial) x 101 (vertical). Although formal grid independence is not claimed, the authors' previous experience with such grids for compression corner flows strongly suggests that the results are close to grid independent. Wall functions for the momentum and turbulence equations have been used to avoid the time consuming computations within the viscous sublayer. This required that the first grid node off the wall lies in the range of $30 \leq y^+ \leq 300$.

3. Steady state results

3.1 Flow structure

A schematic of the inflow conditions and overall flow structure is shown in Fig. 1. The diagram indicates an oblique shock angle of 20.6°, corresponding to the predicted and measured values for this Mach number. Computed contours of the
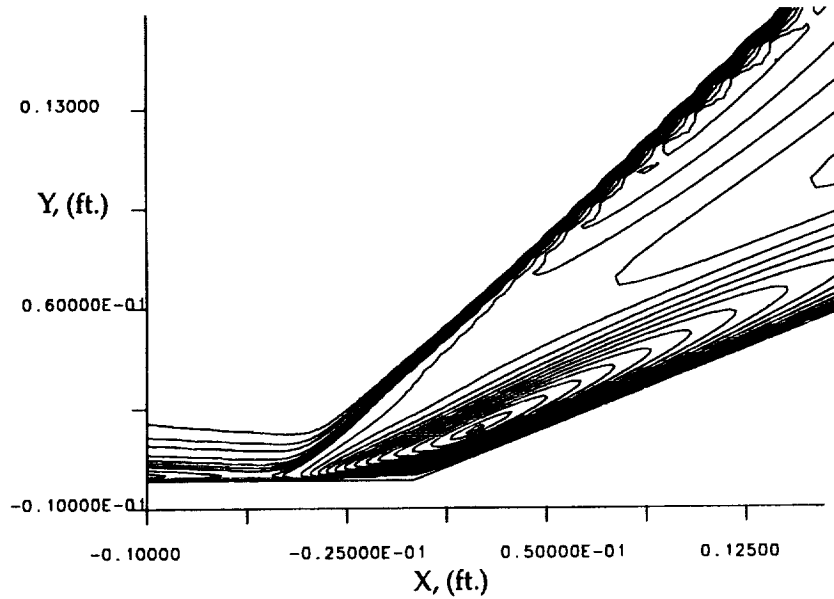
FIGURE 2. Turbulent kinetic energy contours for baseline $k - \epsilon$ model.
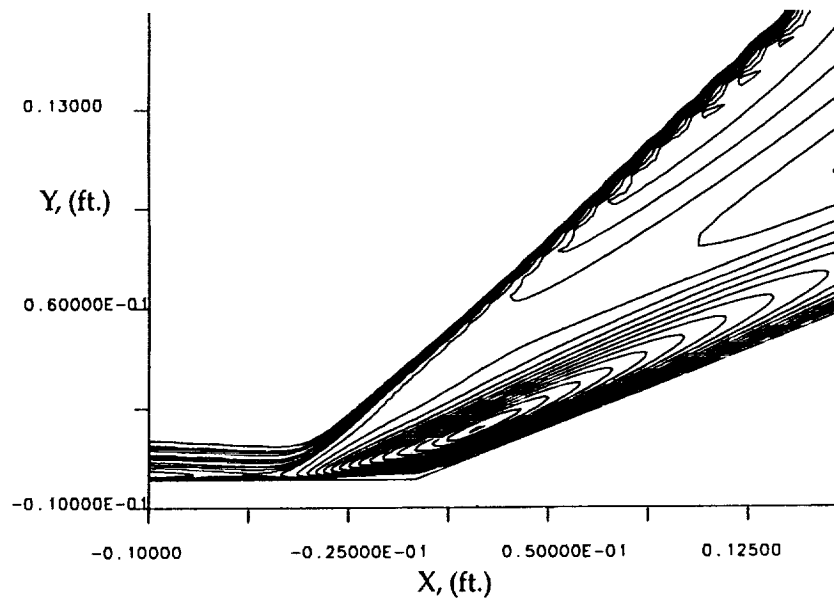

FIGURE 3. Turbulent kinetic energy contours for $k - \epsilon$ with modeled pressure dilatation term.

steady-state turbulent kinetic energy are shown in Figs. 2 and 3. For the baseline $k - \epsilon$ model, Fig. 2, the contour indicates shock formation upstream of the corner, with a strong, intensely turbulent vortex centered just downstream of the corner. The boundary layer redevelops downstream of the shock, with the flow relatively quiescent between the shock and the ramp wall.
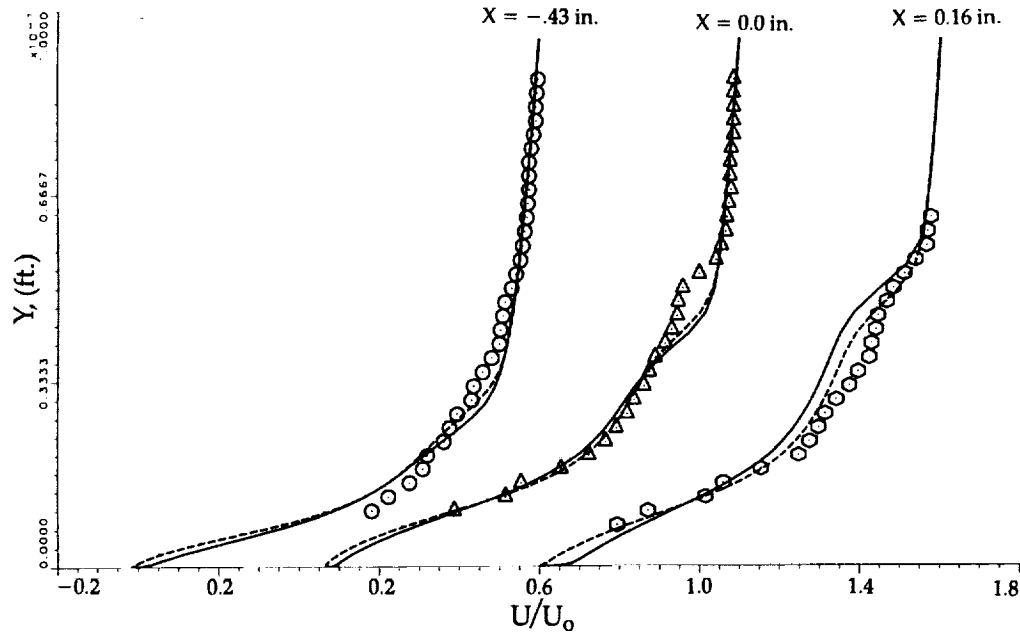
FIGURE 4.   Streamwise velocity profiles in the vicinity of the separation bubble.
o , data; ———— , baseline $k - \epsilon$; ———— , $k - \epsilon$ with pressure dilatation.

The contour showing the compressible flow model results, Fig. 3, indicates a similar flow structure to that of the baseline model. Flow separation begins slightly further upstream in this case, although this is only discernable through detailed post-processing of the results.

3.2 Mean velocity results

Mean streamwise velocity profiles at three key downstream locations are shown in Fig. 4. The locations selected for comparison are near the bubble separation point, the corner, and near the bubble reattachment point. Measurements do not extend all the way to the wall, hence it is difficult to determine exactly where separation begins and what is the magnitude of the reverse flow. In each profile, the model predictions using the pressure dilatation model show minor improvement in the prediction of axial velocity when compared to the baseline $k - \epsilon$ result. The compressible model shows a more rapid adjustment to the inflection of the velocity profile at the shock passage location, while the baseline $k - \epsilon$ model is noticeably more sluggish in its response here.

3.3 Wall static pressure

A comparison of wall static pressures is shown in Fig. 5. Experimental data, the baseline $k - \epsilon$ prediction, and compressible $k - \epsilon$ results using values of -0.004 and -0.006 for the C_{d1} coefficient are shown. The baseline model result (solid line) severely underpredicts the size of the separation region, recovers to the downstream pressure value too rapidly, and misses prediction of the pressure plateau indicative
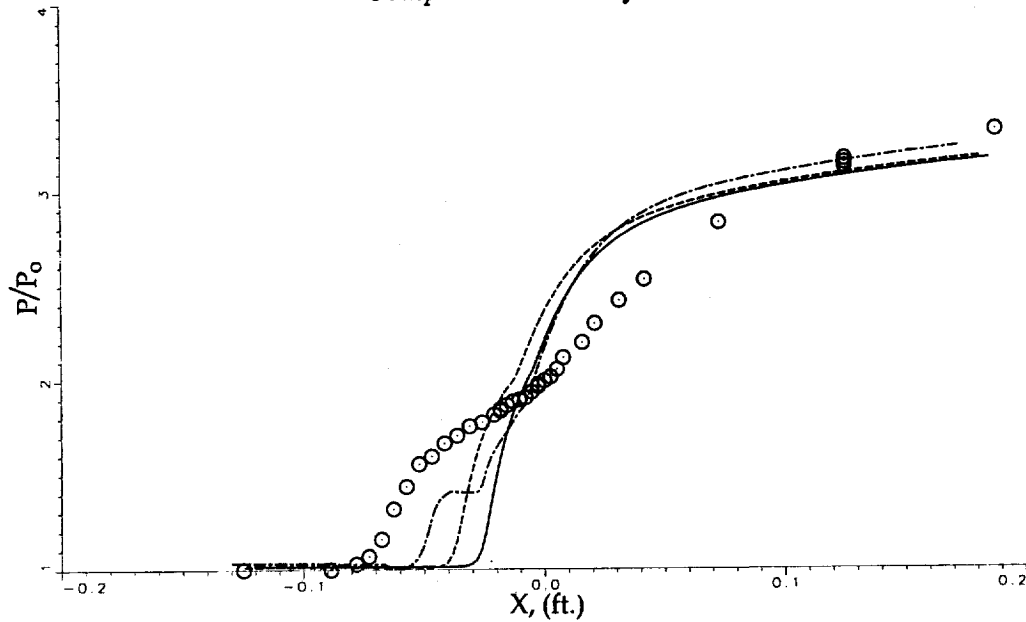
FIGURE 5. Wall static pressure profile. o , data; ——— , baseline $k - \epsilon$; ---- , $k - \epsilon$ with pressure dilatation and $C_{d1} = $ -0.004; $k - \epsilon$ with pressure dilatation and $C_{d1} = $ -0.006,

of the viscous region in flow separation. The compressible $k - \epsilon$ prediction using -0.004 shows an improvement in the upstream region, with pressure lift-off somewhat closer to experimental data, although even this pressure profile is characteristic of weak shock-boundary layer interaction (Delery and Marvin, 1986). As with the baseline case, the pressure plateau is absent, and recovery appears to be too rapid. When a value of -0.006 is used, the pressure plateau indicative of strong interaction has appeared, with the upstream separation point closer to the experimental value.

3.4 Turbulent kinetic energy profiles

The turbulent kinetic energy profiles are shown at a number of downstream locations along the wall and ramp in Fig. 6. As expected from the form of the pressure dilatation model, overall k values are damped at each downstream location for the compressible $k - \epsilon$ model relative to the baseline model. Starting with the profile at the corner, the presence of the shock is noted as a secondary peak in the profile. The shock amplifies the free-stream turbulence significantly; however, it does not quite reach the level of turbulence intensity generated by the wall, even in the strong interaction region immediately downstream of the corner (see Figs. 2 and 3).

4. Unsteady state results

4.1 Unforced boundary layer results

In order to investigate whether the bubble oscillations could be realized simply by running the code in a time-accurate manner, several cases were run in which the global time step was varied from 0.1 second to 10^{-5} seconds. This sampling
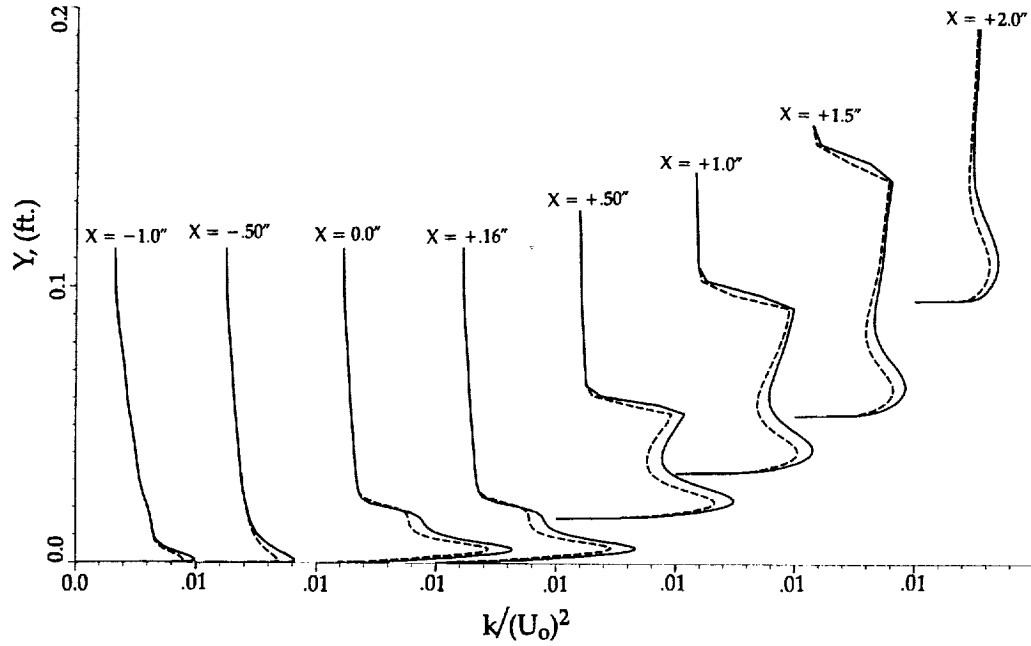
FIGURE 6.   Turbulent kinetic energy profiles at various downstream locations.
—————— , baseline $k - \epsilon$; — — — — , $k - \epsilon$ with pressure dilatation, $C_{d1} = -0.004$.

range was selected as it was estimated that the characteristic bubble frequency for these inflow conditions is approximately 1300 Hz. Monitoring points were installed at multiple locations within the separation bubble to monitor axial and vertical velocity. Over the entire sampling range, negligible bubble oscillations were recorded in the simulations, with no particular resonance at the expected resonant frequency of 1300 Hz. The reasons for the failure to detect the bubble unsteadiness include numerical damping, use of wall functions in the momentum and turbulence equations, or simply the nature of the R.A.N.S. model. As the bubble self-excitation could not be detected, an attempt was made to excite bubble oscillations through perturbation of the inlet boundary layer.

4.2 Forced boundary layer results

In order to excite the bubble into a resonant frequency, an upstream boundary layer perturbation of the form:

$$U(X_o, y, t) = U(X_o, y, 0) + 0.05 U(X_o, y) \sin(\omega t) exp(-5y/\delta)$$

was applied. This provided a single wavelength oscillation whose amplitude decayed effectively to zero at the boundary layer edge. The perturbation amplitude of 5.0 % was approximately equal to the maximum streamwise turbulence intensity in the measured dataset of Smits and Muck (1987). To bracket the expected resonant

frequency at 1300 Hz, forcing frequencies ranging from 200 Hz to 10,000 Hz were run. Each cycle was sampled 50 times. For a free-stream velocity of 1800 ft/sec, the maximum perturbation velocity was +/-90 ft/sec. The average response at several sensing locations in and around the separation bubble is given in the table below:

Forcing Frequency	Peak-to-Peak Amplitude
200 Hz	+/- 0.252 ft/sec
1000 Hz	+/- 0.307 ft/sec
1500 Hz	+/- 0.235 ft/sec
2000 Hz	+/- 0.596 ft/sec
2500 Hz	+/- 0.795 ft/sec
4000 Hz	+/- 0.795 ft/sec
5000 Hz	+/- 0.686 ft/sec
6000 Hz	+/- 0.680 ft/sec
10000 Hz	Divergent

The results indicate that only a very mild separation bubble resonance was computed, in the range of 2500 to 4000 Hz, with lower amplitude of oscillation at lower and higher frequencies. Thus, even with a strong upstream boundary layer perturbation, bubble resonance proved exceptionally difficult to predict.

4.3 Time-scale considerations

The result of the unsteady, forced inflow investigation raises some important issues regarding the resolution of solvers based on R.A.N.S. equations and the k-ϵ model used for prediction of unsteady flow. Some insight into this problem can be gained from a comparison of the governing time scales which characterize the unsteadiness. Here the comparison is drawn between turbulent boundary layer (T.B.L.) oscillations in the supersonic compression corner and bluff-body flow oscillations due to vortex shedding which was successfully modeled by Durbin (1994). In boundary layers, the typical size of the large eddies is order δ, the T.B.L. thickness. Hence, a probe in this region would measure large-eddy frequencies on the order of $f_t \sim U/\delta$, where U is the average speed in the turbulent boundary layer and $U \sim U_\infty$ is the free-stream velocity. From the measurements of Dolling and Or (1993), it is known that the separation bubble oscillation frequency is $f_o \simeq 0.13 U/\delta$, or only 1/7.7 that of the large-eddy frequency. It is noted that these oscillations could not accurately be computed using the R.A.N.S. solver, as described above.

In bluff body dynamics, such as the flow over circular, square, or triangular cylinders, the shedding or Strouhal frequency in the wake region is measured as $f_o \approx 0.2 U_\infty/L$, where $U_\infty =$ free-stream velocity and L is the cross-sectional dimension, the diameter in the case of a circular cylinder. This is true for flows where $Re_D = U_\infty D/\nu \geq 100$. When such cases are run in an unsteady mode using a computational domain with adequate upstream and downstream length (and unsteady boundary conditions, if necessary), vortex shedding of the correct frequency is obtained. We know from the T.B.L. case that the large-eddy frequency at separation

is $f_t \sim U_\infty/\delta$, where δ can be estimated from the relation for flow over circular cylinders as $\delta_o/D \sim 0.16/Re_D^{1/7}$. Thus, for $Re_D \simeq 10^6$, we get $\delta_o/D \sim 0.16/(10^6)^{1/7} \sim 0.0222$. We therefore compute a time-scale ratio of $f_t \ / \ f_o \simeq (10^6)^{1/7}/0.2/0.16 \simeq 224$. Hence, the ratio of turbulence-to-shedding frequencies is $224 \ / \ 7.7 \sim 29.2$.

The *ratio of characteristic frequencies* is thus a key parameter in determining whether R.A.N.S.-type solvers using the standard k-ϵ turbulence model will *resolve* the unsteadiness observed in the experimental data. In the compression corner case, the ratio of $f_t \ / \ f_o$ was found to be only 7.7, while for bluff body flow, the same ratio was found to be 224 at $Re_D = 10^6$, nearly 30 times greater than that for the compression corner. Based on the limited data, it appears that for f_t/f_o of order 1, turbulence-driven oscillations will be submerged in the turbulence model and prove difficult to resolve. Unsteady turbulence models which adjust properly to both temporal and spatially local flow conditions may be necessary to resolve this level of unsteadiness. Large-scale or momentum-driven oscillations of order $f_t/f_o \sim 100$ or greater should be relatively easy to compute using unsteady R.A.N.S. solvers, with the selection of turbulence model not nearly as important in these cases. For the large body of cases which fall in between these two extremes or for cases which exhibit multiple levels of unsteadiness such as the rotational, supersonic flow in gas turbine compressors, a more critical analysis of the importance of time scales involved and the underlying turbulence model is necessary.

5. Conclusions

The results indicate that the compressibility correction term represented by the pressure dilatation model of Zeman (1991) improves the velocity profiles predictions in the vicinity of the separation bubble to a small degree. Wall pressure predictions were also slightly improved. The term generally had the effect of damping turbulent kinetic energy as was seen in a series of k profiles at various downstream locations. Increasing the value of the modeled coefficient C_{d1} from -0.004 to -0.006 had the effect of increasing the separation bubble size, resulting in a form of the pressure plateau reported in the steady-state wall pressure results for ramp angles of 20° or greater at $M_\infty = 2.84$. Unsteady runs with and without upstream boundary layer perturbations did not predict the measured separation bubble oscillations. An analysis of the characteristic time scales for this problem revealed that the expected bubble oscillation frequency was less than the characteristic large-eddy frequency, which proved numerically difficult for the R.A.N.S. solver and k-ϵ model to resolve. It was postulated that the condition $f_t/f_o \gg 1$ must be met for the code to easily compute unsteadiness in the flow. An example from bluff body dynamics was used to illustrate this point.

<div style="text-align:center">REFERENCES</div>

DELERY, J. & MARVIN, J. G. 1986 Shock-wave boundary layer interactions. *AGARD Report 280.*

DOLLING, D. S. & OR, C. T. 1983 Unsteadiness of the shock wave structure in attached and separated compression ramp flowfields. *AIAA Paper 83-3720.*

DURBIN, P. A. 1994 Separated flow computations with the $k - \epsilon - v^2$ turbulence model. *CTR Manuscript 152.* Also, to appear in *AIAA Journal.*

DURBIN, P. A. & ZEMAN, O. 1992 Rapid distortion theory for homogeneous compressed turbulence with application to modeling. *J. Fluid Mech.* **242**, 349-370.

HINZE, J. O. 1975 *Turbulence.* McGraw-Hill, New York.

HORSTMAN, C.C. 1987 Prediction of hypersonic shock wave/turbulent boundary layer interaction flows. *AIAA Paper 87-1367.*

JONES, W. P. & LAUNDER, B. E. 1972 The prediction of laminarization with a two-equation model of turbulence. *Int. J. Heat Mass Transfer.* **15**, 301-314.

MARVIN, J. G. 1991 Baseline Models for Turbulence Compressibility Studies. *NASP/NASA Ames GWP #18 Workshop on Turbulence Compressibility.*

SMITS, A. J. & MUCK, K.-C. 1987 Experimental study of three shock wave/ turbulent boundary layer interactions. *J. Fluid Mech.* **182**, 291-314.

VANDROMME, D. & ZEMAN, O. 1992 Response of a supersonic boundary layer to a compression corner. *Proc. of the Summer Program.* Center for Turbulence Research, NASA Ames/Stanford University. 247-258.

ZEMAN, O. 1991 Dilatation dissipation: The concept and application in modeling compressible mixing layers. *1991 Annual Res. Briefs.* Center for Turbulence Research, NASA Ames/Stanford University, 1991, 105-117.

ZEMAN, O. & COLEMAN, G. N. 1991 Compressible turbulence subjected to shear and rapid compression. *Turbulent Shear Flows 8.* Springer Verlag.